An improved contact method for quantifying the mixing of a binary granular mixture

Papapetrou, T. N.; Lecrivain, G.; Bieberle, M.; Boudouvis, A.; Hampel, U.;

Originally published:

January 2021

Granular Matter 23(2021), 15

DOI: https://doi.org/10.1007/s10035-020-01073-3

An improved contact method for quantifying the mixing of a binary granular mixture

Theodoros Nestor Papapetrou,[1,2] Gregory Lecrivain,[2] Martina Bieberle,[2] Andreas Boudouvis,[3] Uwe Hampel[1,2]

[1] Technische Universität Dresden, Institute of Power Engineering, Chair of Imaging Techniques in Energy and Process Engineering, Dresden, Germany
[2] Helmholtz-Zentrum Dresden-Rossendorf, Institute of Fluid Dynamics, Bautzner Landstraße 400, 01328 Dresden, Germany
[3] National Technical University of Athens, School of Chemical Engineering, Athens, Greece

Corresponding authors: t.papapetrou@hzdr.de, g.lecrivain@hzdr.de

Declarations
Funding
Funded within the Saxon State Scholarship by the Free State of Saxony.

Conflicts of interest/Competing interests
The authors declare no conflict of interests.

Availability of data and material
The image sequence used in this work is available in the supplementary material.

Code availability
The implementation of the variance and modified contact methods will be made accessible with a DOI number after an embargo period, that is when the manuscript is accepted for publication.

Authors' contributions
T.N.P. performed the experiments, designed and implemented the method. G.L., M.B., and U.H. supervised the project. All authors analyzed the data and wrote the manuscript.

Acknowledgements
This work was supported by a “Landesstipendium” awarded by the Graduate Academy of the Technische Universität Dresden.

Abstract
When two granular phases are brought into motion in a rotating drum, a competition of mixing and segregation occurs. Several image analysis methods have been used to quantify the mixing. In this work, a modification of the contact method, originally proposed by Van Puyvelde (1999), is suggested to allow evaluation of the mixing index for each separate image. A strength of this modified method lies in the removal of the case-dependent normalization of the mixing index, which has so far impaired a direct comparison to other studies. This modified method is tested on artificial and experimental images of a granular bed composed of spherical glass and polypropylene beads of equal size. The bed evolves in a rotating drum under the rolling regime. The temporal evolution of the mixing index is in excellent agreement with the commonly used variance method.

Keywords
Binary particle mixing, rotating drum, image analysis, mixing index, contact method, variance method.

1. Introduction

The mixing of granular species in a rotating system is found in many industrial applications, such as in the pharmaceutical, food, metallurgical, and plastic industries. In such processes, mixing is needed for coating [1], drying [2], heating [3, 4], or chemical reaction of granules [5]. The primary goal of mixing is to achieve a homogeneous granular mixture. Differences in granular properties, such as particle size, shape or density, result however in complex segregation dynamics [6–8]. In a rotating cylindrical drum without baffles, the simplest and most widely studied geometry, both radial and axial segregation occur. The radial segregation [8, 9], which is of primary interest here, occurs shortly after the drum is set into motion, typically within one to three rotations [10]. Axial segregation, on the other hand, develops over a much larger time scale [11, 12]. Experimental techniques used to investigate the temporal formation of segregation zones include high-speed cameras [10, 13], bed freezing, slicing and reconstruction [7], and magnetic resonance imaging [11]. In addition, the mixing can also be studied with computer simulations [13–16]. In all these methods, images taken either at the front end of the drum or across the granular bed are analyzed to characterize the mixing as a function of the time t. The quality of the mixture is normally quantified by a dimensionless parameter $M(t)$, known as the mixing index varying between zero and unity, with $M = 0$ indicating a perfectly segregated state and $M = 1$ a perfectly mixed state [7, 17]. Various formulations of the mixing index have been suggested for experimentally sampled mixtures [18, 19], as well as for simulated mixtures [20–23]. With respect to image analysis, two methods have been proposed to estimate the temporal evolution of $M(t)$, namely the variance and the contact method.

Lacey [17, 24] pioneered the field by suggesting a mathematical formulation of the mixing index for a binary granular mixture with a uniform particle size distribution. Originally, M was calculated using the statistical variance (σ^2) defined in a system at rest as

$$\sigma^2 = \frac{1}{N-1}\sum_{k=1}^{N}(c_k - \bar{c})^2, \tag{1}$$

where c_k is the local concentration of the reference granular species in the k-th sample, N the number of samples containing exactly n manually extracted particles, and $\bar{c}$ the overall concentration of the reference granular species. The mixing index was suggested as

$$M = \frac{\sigma_{\max}^2 - \sigma^2}{\sigma_{\max}^2 - \sigma_{\min}^2}, \tag{2}$$

with $\sigma_{\max}^2 = \bar{c}(1-\bar{c})$ and $\sigma_{\min}^2 = \sigma_{\max}^2/n$. The variance method was later extended to calculate the temporal evolution $M(t)$ out of an image sequence [10, 13]. In those studies, the samples were obtained by discretizing each image into squares or pie-like windows [7, 16]. A disadvantage of the variance method lies in the fact that the mixing image is strongly dependent on the window size. A small window gives the overall impression of a bad mixing, while a larger window that of a good mixing [19].

Van Puyvelde et al. [25] originally introduced the contact method to investigate the heat transfer across a granular bed being mixed in a rotary kiln. The mixing was quantified by converting the number of contacts between two adjacent pixels of different colors into an interfacial contact length (L_c). A greater contact length means a better mixing. Chou et al. [26] developed a similar method by looping through all first-species particles and counting the number of neighboring second-species particles. In similar studies on binary mixing [27, 28], where the particles only differed in color, the number of contacts (C) had been converted into a mixing index as

$$M(t) = \frac{C(t) - C_{\min}}{C_{\max} - C_{\min}}, \tag{3}$$

where $C_{\min}$ was the number of contacts calculated in the initial segregated state at time $t = 0$ and $C_{\max}$ the maximum number of contacts calculated from the entire image sequence. The contact method has disadvantages too. First, Eq. (3) can theoretically attain negative values if the initial state is not perfectly segregated. Second, comparison with other studies is made difficult by the fact, that each experimental image sequence has its own minimum and maximum numbers of contacts $C_{\min}$ and $C_{\max}$. Both the variance method and the contact method have shown to provide quantitatively similar results in terms of mixing index. Yet a suitable normalization, often case-dependent, must be chosen for $C_{\min}$ and $C_{\max}$ [28], making in-turn the contact method rather unattractive. In this work, a modified contact method is proposed, thus enabling comparison between different granular systems, while keeping a reduced dependency on subjective parameters.

2. Materials and methods

2.1. Experimental setup

The experimental setup consists of a horizontal cylindrical PMMA drum with a length of 1 m and an inner diameter of 144 mm. The particle bed evolved in the front 30 centimeters of the inner cylinder delimited by a back PVC wall and a front PMMA cap. The back end of the cylinder was mounted on a motor. The inner cylindrical and the back delimiting surfaces of the drum were coated with aluminum spray and grounded to evacuate the static charge, while the inner front cap was sprayed with a transparent antistatic spray. Initially, equal bulk volumes of white glass spherical beads (diameter: 4±0.3 mm, density: 2.5 g/cm^3) and red polypropylene spherical beads (diameter: 3.97±0.13 mm, density: 0.9 g/cm^3) were placed in the drum in a side-by-side arrangement with a granular filling set to 35% of the drum volume. The white particles occupied the left half and the right particles the right half. The drum rotated counterclockwise with a speed of 30 rpm for 40 seconds. A Mega Speed HHC X7 High Speed Camera captured the particles from the transparent front cap with 25 frames per second.

2.2. Image pre-processing

Hereafter, red, white, and black are respectively associated with polypropylene, glass, and the background of the image. The pre-processing part is necessary to turn each image into a ternary two-dimensional field, where only red, white and black areas co-exist. To this end, a field $\mathbf{F}(x, y)$ taking the value 0 in the background, 1 in the red constituent, and 2 in the white constituent is introduced. The field $\mathbf{F}$ can be precisely defined using simulation data, for instance with the discrete element method [29]. In the case of experimental images, $\mathbf{F}$ is approximated by a two-dimensional matrix $\mathbf{P} = \{P_{i,j}\}$. In each image, every pixel is classified as black, red or white as follows. First, two intermediate matrices for the red, $\mathbf{K} = \{K_{i,j}\}$, and white colors, $\mathbf{Q} = \{Q_{i,j}\}$, with $K_{i,j}$ and $Q_{i,j}$ equaled to either zero or unity, are created using appropriate thresholds as

$$K_{i,j} = \begin{cases} 1 & \text{if} \quad H_{i,j} \geq T_{H1} \text{ and } H_{i,j} \leq T_{H2} \text{ and } R_{i,j} \geq T_R \quad \text{red} \\ 0 & \text{elsewhere} \quad \text{not red} \end{cases} \tag{4}$$

and

$$Q_{i,j} = \begin{cases} 1 & \text{if} \quad S_{i,j} \leq T_S \text{ and } V_{i,j} \geq T_V \quad \text{white} \\ 0 & \text{elsewhere} \quad \text{not white} \end{cases} \tag{5}$$

where $R_{i,j}$ is the RGB value of the red channel of the (i, j)-th pixel, $H_{i,j}$, $S_{i,j}$, $V_{i,j}$ the HSV values of the (i, j)-th pixel, and T_{H1}, T_{H2}, T_R, T_S , T_V the thresholds. The exact threshold values depend on the lighting conditions of the experiment and were determined using the Color Thresholder implemented in Matlab. Next, the noise present in the matrices $\mathbf{K}$ and $\mathbf{Q}$ originating from the lighting effects is eliminated. This is achieved by applying a series of three erosions followed

by three dilations using a square 3×3 matrix containing 1 everywhere as a structuring element [30]. The resulting noise-free matrices $\mathbf{K}'$ and $\mathbf{Q}'$ are then combined into a new matrix $\mathbf{P}' = \{P'_{i,j}\}$ defined as $\mathbf{P}' = \mathbf{K}' + 2\mathbf{Q}'$. For each pixel, $P'_{i,j}$ takes the values 0, 1, 2, or 3. For the spurious case, $P'_{i,j} = 3$, the pixel is considered both red and white by the algorithm. The value is therefore corrected by automatically replacing it with the color index, 1 or 2, depending on the most frequent color observed in the neighboring pixels. This concludes the construction of the matrix $\mathbf{P}$. The pre-processed image sequence can be seen in the supplementary material. An extracted image separated manually by the authors into red and white and black is later considered in the result section for comparison purposes.

The red species is hereafter taken as the reference species. The overall time-dependent and space-averaged concentration of red color ($\bar{c}$) is a necessary quantity needed in both the variance method and modified contact method. It is defined for each image as

$$\bar{c}(t) = \frac{A_R}{A_R + A_W}, \tag{6}$$

where A_R and A_W are the areas colored in red and that in white, respectively. If simulation data are used, $\bar{c}$ can be calculated directly from the original field $\mathbf{F}$. With experimental images, as is the case here, $\bar{c}$ is calculated as $\bar{c} \approx N_R/(N_R + N_W)$, where N_R and N_W are the total number of red and white pixels in the image, respectively.

2.3. Variance method

The present method is a modification of that reported by References [13, 28]. The modification is in essence similar to that used by Qi et al. [31]. Each image is divided into a number (N_s) of square windows with length (L). Figure Fig**. 1** shows an artificial image representing the initial segregated state, that is at time $t = 0$ s.

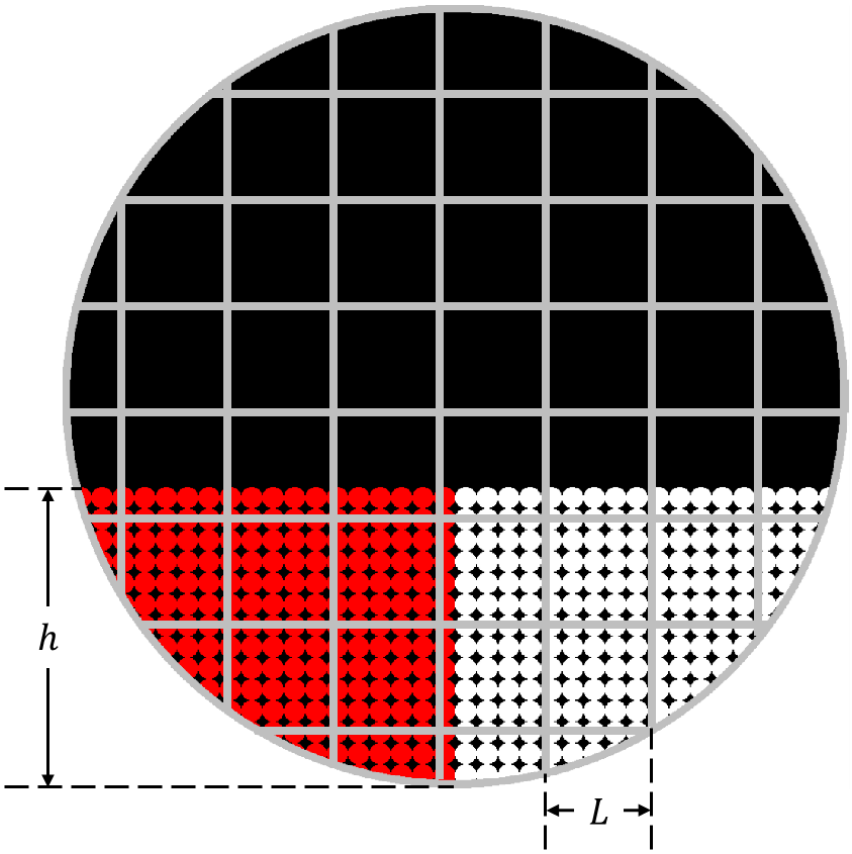

Fig. 1 *Arbitrary discretization of an artificial image into a number (N_S) of square windows with given size (L). The filling height (h) is also shown*

Within the k-th window, a local concentration (c_k), representing the ratio of the reference area to the granular area is first calculated as

$$c_k = \frac{(A_R)_k}{(A_R)_k + (A_W)_k}, \tag{7}$$

where $(A_R)_k$ and $(A_W)_k$ are respectively the red and white areas in terms of pixel numbers in the k-th window. A local weight (w_k), indicating the local fraction of the granular area in the window, is then calculated as

$$w_k = \frac{(A_R)_k + (A_W)_k}{L^2}. \tag{8}$$

By taking into account the local granular weight (w_k) and the local red-to-granular concentration (c_k) in each window, Eq. (1) is conveniently recast as

$$\sigma^2 = \frac{1}{W}\sum_{k=1}^{N_s} w_k (c_k - \bar{c})^2, \tag{9}$$

with the denominator $W = \sum w_k = (A_R + A_W)/L^2$. Some authors [10, 13, 32] have used the denominator $(W - 1)$ in Eq. (9), which is reminiscent of the sample variance formula [33]. In the present case, the overall concentration $\bar{c}$ is however known before each image is discretized. Hence we decided to use a formulation reminiscent of the population variance formula [34]. In practice, W achieves relatively high values. Our tests showed that the choice of the denominator only had a negligible influence on the resulting mixing index given in Eq. (2). Because the window length L is in reality larger than the particle diameter, it is fair to assume $\sigma_{min}^2 / \sigma_{max}^2 \to 0$ [16, 31]. The mixing index in Eq. (2) then simplifies to

$$M = 1 - \frac{\sigma^2(t)}{\sigma_{\max}^2(t)}, \tag{10}$$

with $\sigma_{\max}^2 = \bar{c}(1 - \bar{c})$. In Reference [16], the mixing index was calculated using the square root of the variance as $M = 1 - \sigma/\sigma_{\max}$. Care should be taken, as removing the square operator in Eq. (10) was found to affect the results quite significantly.

2.4. Original contact method

In the original contact method [25, 27, 28], the mixing index is calculated by counting the total number of contacts between red and white pixels. For the sake of simplicity, let us assume two adjacent row matrix elements, $P_{i,j}$ and $P_{i+1,j}$. A contact exists whenever $P_{i,j} + P_{i+1,j} = 3$ (see Figure Fig**. 2**). This contact identification procedure also applies to adjacent column matrix elements, that is $P_{i,j} + P_{i,j+1} = 3$.

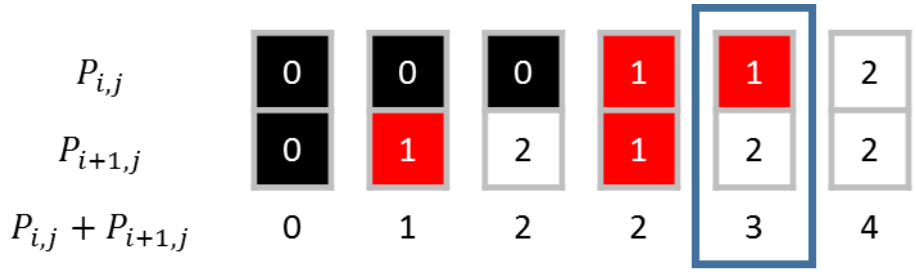

Fig. 2 *All possible combinations of two adjacent pixels. A contact exists whenever* $P_{i,j} + P_{i+1,j} = 3$

Given an image sequence of the binary granular mixture in the rotating drum, the mixing index is calculated using Eq. (3) with $C_{\min}$ and $C_{\max}$ the absolute minimum and maximum in the time sequence, respectively.

2.5. Modified contact method

In this section, a modification of the contact method is suggested to theoretically determine the modified contact lengths $\tilde{L}_{\min}(t)$ and $\tilde{L}_{\max}(t)$ directly from each individual image instead. The mixing index hence becomes

$$M(t) = \frac{\tilde{L}_c(t) - \tilde{L}_{\min}(t)}{\tilde{L}_{\max}(t) - \tilde{L}_{\min}(t)}, \tag{11}$$

where $\tilde{L}_c(t)$ is the modified contact length also calculated for each image in the sequence. The automated pre-processing stage may lead to interstitial background between two particles that would normally be in contact. The original contact method fails to recognize such contacts. See for instance Figure **Fig. 3**a, where a white particle is surrounded by two red particles. By shifting all background elements to the right, a modified contact length equal to $\tilde{L}_c = 2d_p$ can be conveniently calculated for the centered white particle.

Fig. 3 *The interstitial background between particles seemingly in contact is bypassed by shifting all black pixels to the right*

The following method is therefore suggested for more intricate images. First, a number of horizontal contacts is calculated by shifting all black pixels in each original image to the far right (Fig. 4b). The procedure is then repeated on each original image by shifting all black pixels downwards and by subsequently counting the number of vertical contacts (Fig. 4c). The sum of horizontal and vertical contacts is the new number of modified contacts $\tilde{C}$ and, after conversion, it becomes the modified contact length $\tilde{L}_c$.

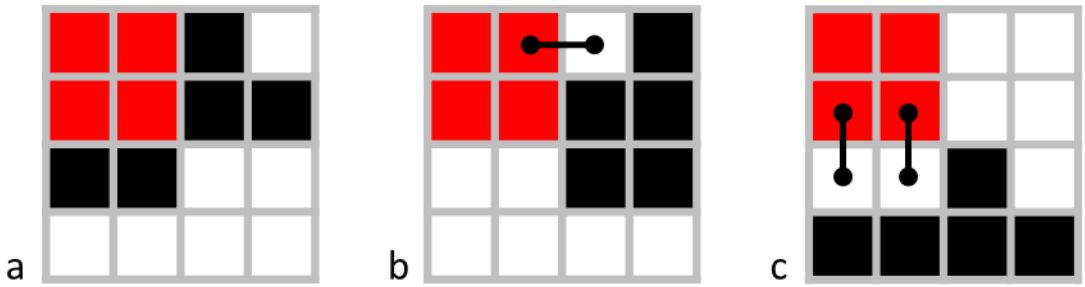

Fig. 4 *Example of an image sample with no original contacts (a). After shifting all black pixels to the right, one horizontal contact exists (b). After shifting all black pixels downwards, two vertical contacts exist (c). In total there are $\tilde{C} = 3$ modified contacts*

To compute the minimum contact length ($\tilde{L}_{\min}$), a theoretical redistribution of the granular field into a fully segregated state as illustrated in Figure Fig**. 5** is considered, with $\tilde{L}_{\min}$ corresponding to the height of the segregating straight line. First, the free surface is fitted with a straight line using the linear least-squares method and the drum with a circle using the method by Pratt [35]. The largest distance from the fitted line to the bottom of the granular bed,

indicated here by $\tilde{h}$, corresponds to the modified filling height. Our results presented in Appendix A show, that the modified height ($\tilde{h}$) slightly fluctuates over time with a mean value close to the initial height $h(t=0)$. The modified granular area below the fitted line is given by $\tilde{A} = \tilde{D}^2[\tilde{\varphi} - \sin\tilde{\varphi}]/8$, where $\tilde{D}$ is the fitted drum diameter and $\tilde{\varphi} = 2\cos^{-1}(1 - 2\tilde{h}/\tilde{D})$ the modified filling angle defined at the drum center. The minimum contact length is calculated as

$$\tilde{L}_{\min} = \tilde{h} - \frac{\tilde{D}}{2} + \sqrt{\tilde{\ell}(\tilde{D} - \tilde{\ell})}, \tag{12}$$

where the modified length ($\tilde{\ell}$) illustrated in Figure **Fig. 5** is obtained by solving the following equation

$$\tilde{A}_R(\tilde{\ell}) = \bar{c}\tilde{A}. \tag{13}$$

The modified red area ($\tilde{A}_R$), plotted as a function of the modified length ($\tilde{\ell}$) in **Fig. 6**, is further detailed in Appendix B. The right-hand side ($\bar{c}\tilde{A}$) of Eq. (13) is the modified reference area. Because of trigonometric functions, a gradient-based method is used to solve present Eq. (13)

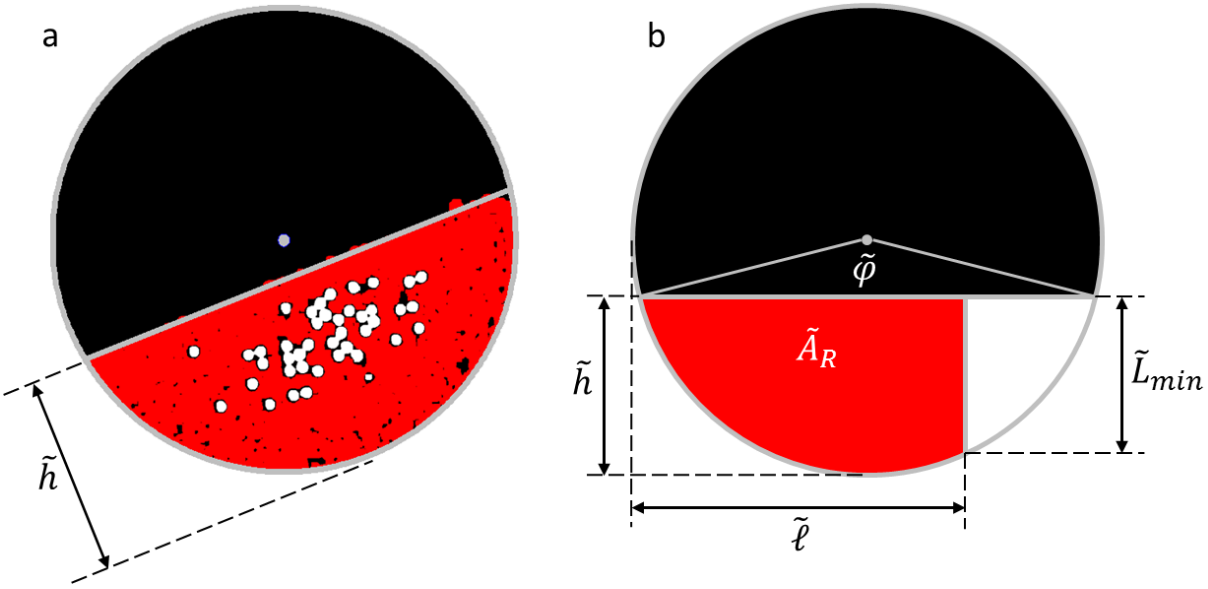

Fig. 5 *Schematic representation of the calculation of $\tilde{L}_{min}$. First, the free surface is fitted with a straight line and the bed height ($\tilde{h}$) is calculated (a). Then the granular species are distributed inside the bed area (b)*

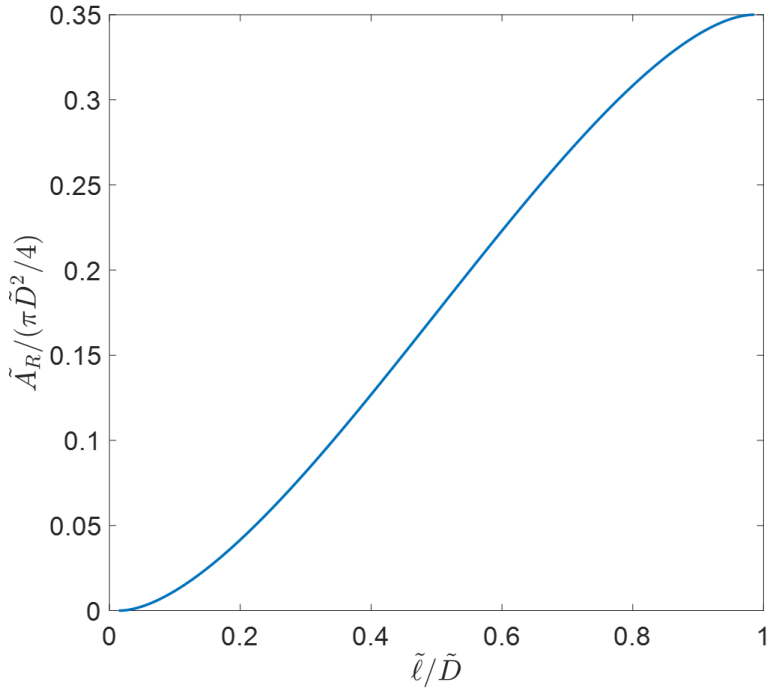

Fig. 6 *The modified red area ($\tilde{A}_R$) as a function of the modified length ($\tilde{\ell}$) for the modified height ($\tilde{h}$) corresponding to the experimental filling degree, 35% of the drum volume*

To compute the maximum contact length ($\tilde{L}_{\max}$), let $A = A_R + A_W$ be the granular area in the image and $A_p = \pi d_p^2/4$ the projected area of a single particle. The granular area (A) is here calculated using the pixel number and, hence, differs from that mathematically defined previously ($\tilde{A}$). The area (A_p) could also be estimated by counting the corresponding pixel number. The ratio (A/A_p) approximates the total particle number in the image and $A/A_p \min(\bar{c}, 1-\bar{c})$ the particle number of the rarest granular species. The greatest modified contact length that can be possibly achieved for any single particle is $4d_p$, that is when a particle of the rarest species is surrounded by four particles of the other species positioned at all cardinal positions (see **Fig. 7**).

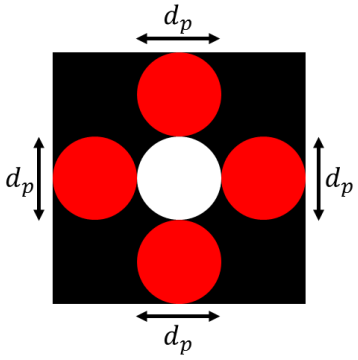

Fig. 7 *Illustration of the maximum possible number of modified contacts*

Further particle arrangements are in fact possible and will lead to an identical formulation. An estimation of the maximum contact length is therefore given by

$$\tilde{L}_{\max} = 4d_p \frac{A}{A_p} \min(\bar{c}, 1-\bar{c}). \tag{14}$$

3. Results and discussion

3.1. Artificial images of an ideally mixed particle bed

As illustrated in **Fig. 8**, the modified contact method is first tested on a set of four individual artificially made images exhibiting an ideal mixing.

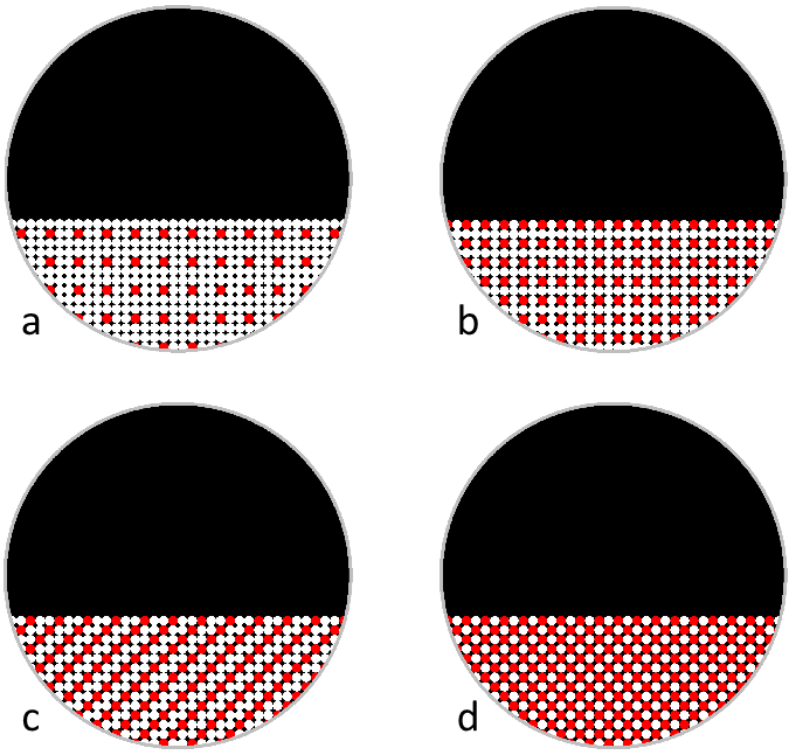

Fig. 8 *Artificial images of perfect mixing made with increasing red concentration set to* $\bar{c} \approx 0.11$ *(a),* $\bar{c} \approx 0.25$ *(b),* $\bar{c} \approx 0.33$ *(c), and* $\bar{c} \approx 0.50$ *(d)*

The mixing indices, respectively calculated with the variance method and with the modified contact method, are provided in Table 1. For comparison purposes, the variance method was employed with two typical window sizes, namely $L = 3d_p$ and $L = 4d_p$ [28]. Unlike our modified contact method, the variance method does not deliver a single value for the mixing index, but a range of values. The minimum and maximum of each range in given below.

Tab. 1 *Comparison of the variance method (Eq. (10)) with the modified contact method (Eq. (11)), applied on artificial images with increasing concentration* $\bar{c}$

Image	$\bar{c}$	Mixing index (M)		
		Eq. (10) $L/d = 3$	*Eq. (10)* $L/d = 4$	*Eq. (11)* -
Fig. 8a	0.11	0.94 - 1.00	0.93 - 0.99	0.98
Fig. 8b	0.25	0.88 - 1.00	0.96 - 1.00	0.94
Fig. 8c	0.33	0.98 - 1.00	0.98 - 1.00	0.96
Fig. 8d	0.50	0.97 - 1.00	1.00	0.97

The results show that the modified contact method consistently gives values higher than 0.94, reflecting the perfectly mixed state. This value agrees well with the mixing index range delivered by the variance method. Note that the results from the original contact method are not listed in the table. The reason behind is that a minimum and a maximum number of contacts

cannot be given for single images but only for an image sequence, thereby illustrating the strength of the suggested modification.

3.2. Realistic images

In this section, the modified contact method is anew tested on images that are more realistic. In **Fig. 9**, image (a) represents a perfectly initial segregated state, (b) a perfectly mixed organized state, and (c) an ideal segregated state reminiscent of the steady state eventually achieved in the drum. Images (a), (b), and (c) were constructed the with same filling height (h) and the same reference concentration $\bar{c} \approx 0.50$. Image (d) is taken from the real experimental sequence, (e) was obtained after the automatic pre-processing, and (f) after a manual pre-processing performed by the authors. In images (e) and (f), the reference concentration is calculated as $\bar{c} \approx 0.9$.

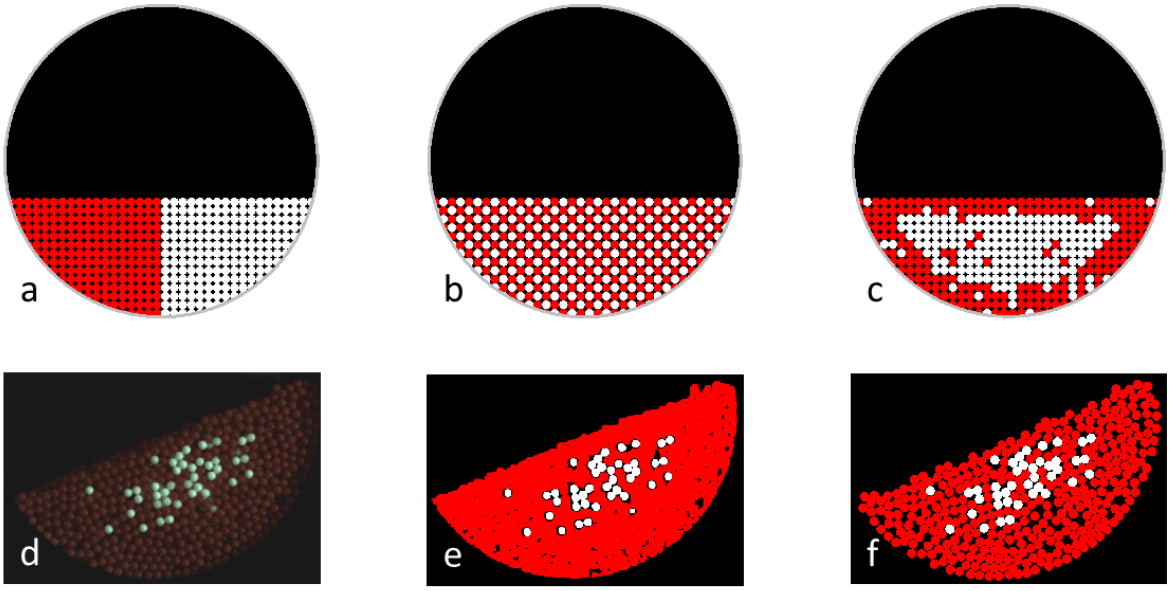

Fig. 9 *Tested images: (a) ideal segregation, (b) ideal mixing, (c) ideal steady-state mixing; (d) experimental image, (e) automatically pre-processed image using algorithm described in section 2.2, and (f) manually pre-processed image*

At first, the variance method is applied to the images (a), (b), (c), (e) and (f). The results are shown in **Fig. 10**. In his section, the effects of the window size and the grid position are also examined. For each image, the mixing index is shown as a function of the window size L varying between 1 pixel and $6d_p$. For a given window size (L), there are L^2 possible grid positions, leading to L^2 values of the mixing index. The minimum and maximum of these values are plotted as enveloping curves in **Fig. 10**, where the abscissa (L/d_p) has been normalized with the particle diameter. The mixing index obtained with our modified contact method was calculated as well. Its values are depicted as straight blue lines, since they do not depend on the window size (L).

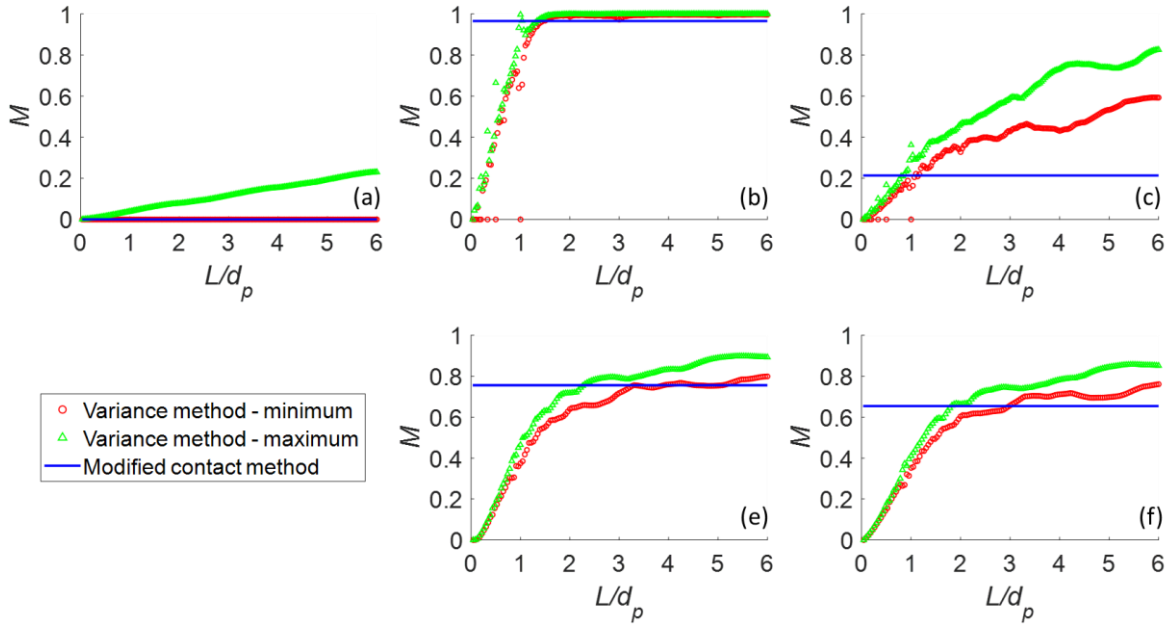

Fig. 10 *The minimum and maximum values of the mixing index obtained with the variance method (Eq. (10)) as a function of the window size (L/d_p) are depicted as points. The mixing index obtained with the modified contact method is depicted as a solid horizontal line*

It can be seen in Fig. **10** that the modified contact method agrees in most static scenarios with the variance method. Image (a) exhibits a mixing index close to zero and image (b) close to unity, as expected. The other three images (c, e, and f) exhibit intermediate mixing indices, which is also as expected. All these images clearly show the effects of the window size and grid position, inherent to the variance method, on the mixing index calculation. In each image, two enveloping curves are formed showing the minimum and maximum values taken by the mixing index. The difference between the two extreme values does not seem to decrease as L/d_p increases, suggesting there is no sufficiently large L for which these two values converge. In all scenarios, the enveloping curves start from zero, because the system looks completely segregated at that pixel scale. In fact, a window size $L/d_p < 1$ has no real physical meaning, because the sample size is simply too low to reflect the mixing occurring at a scale larger than the particle diameter. As a rule of thumb, a window size greater than $L/d_p > 2$ is normally suggested in the literature [28]. The results also suggest that the proposed automatic pre-processing (e) is sufficient, since it gives results comparable to those obtained with the manually segmented image (f). The two mixing indices calculated by the modified contact method in images (e) and (f) are very close to each other. The difference falls below 11%. When compared to the variance method in the region $2 < L/d_p < 3$, a typical window size cited in the literature [28], a good agreement is also achieved for images (e) and (f). A maximum difference of about 12% is typically observed between the two methods. In image (c), the mixing index obtained with our modified contact method does not compare as well with that from the variance method in the region of interest, that is $2 < L/d_p < 3$. This can probably be attributed to the white granular core that is much more compact in image (c) than in images (e) and (f).

With respect to conclusions so far drawn on the variance method, only the enveloping curves have been addressed. **Fig. 11** illustrates the distribution of the in-between mixing indices in the form of histograms. In total, three different window sizes are tested. The relative frequencies of M obtained from the experimental image (e) suggest that there is no natural way to choose a representative value. On the one hand, the three histograms clearly do not exhibit a similar distribution. On the other hand, neither a Gaussian nor a uniform distribution can be observed, making it in-turn more difficult to choose a representative mixing index. Our modified contact method overcomes these two shortcomings.

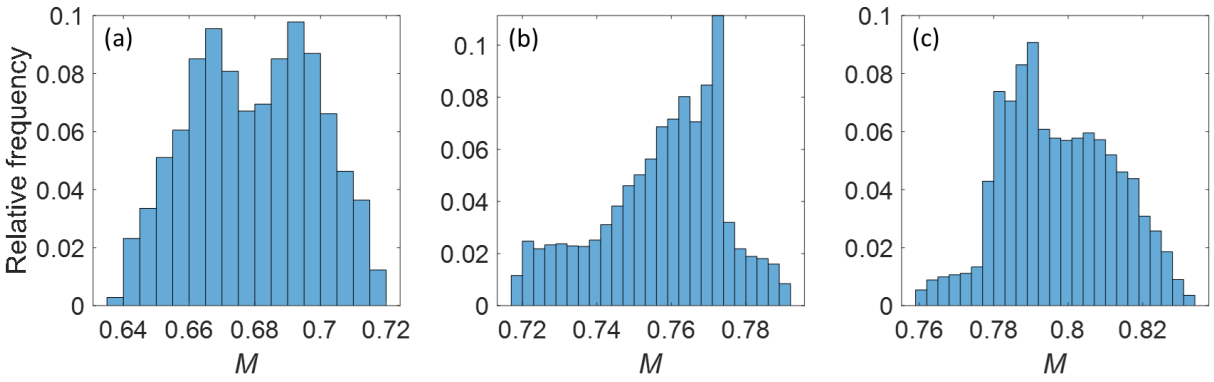

Fig. 11 *Relative frequency for the mixing index obtained with the variance method applied to image (Fig. **9**e). The values are sampled from all possible grid positions. Three window sizes are tested (a)* $L/d_p = 2$*, (b)* $L/d_p = 3$*, (c)* $L/d_p = 4$

3.2. Experimental image sequence of the rotating drum

In this section, the improved contact method is applied to the sequence of experimental images available in the supplementary materials. After some time, the white particles concentrate in the center and are surrounded by a circular band of mostly red particles (See **Fig. 9**d). **Fig. 12** shows the mixing index as a function of time. For comparison purposes, the two enveloping curves obtained with the variance method are also shown. The window size is here set to $L/d_p = 3$.

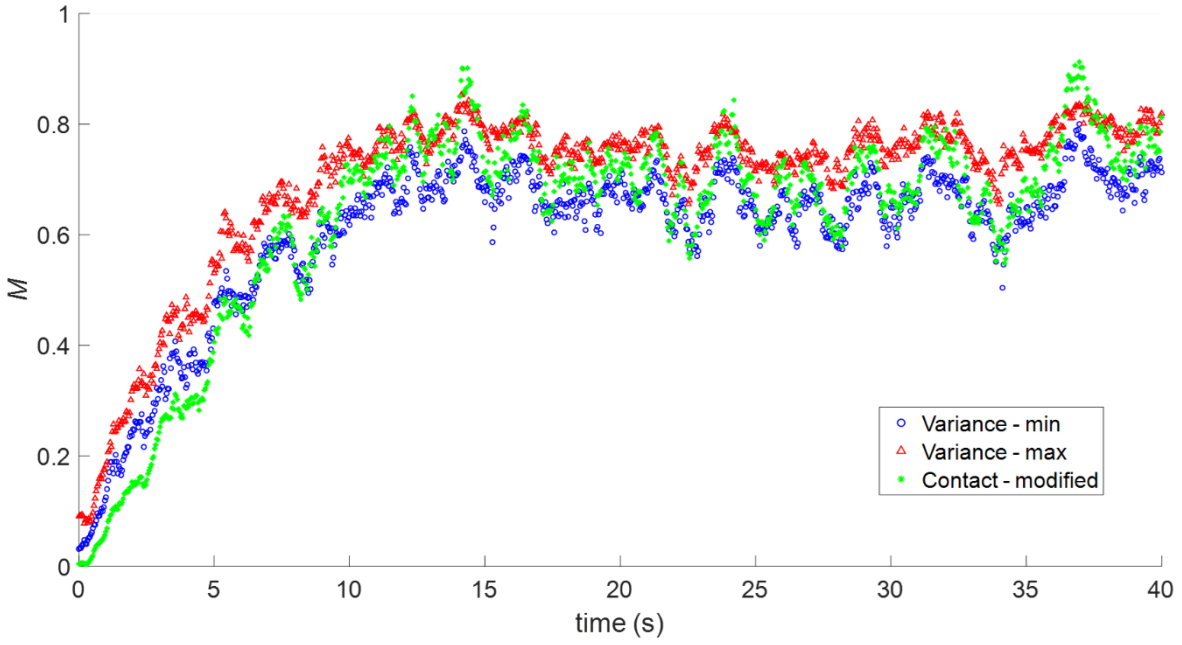

Fig. 12 *The mixing index as a function of time for the various methods*

Throughout the entire sequence, the results from the modified contact method match remarkably well with those obtained with the variance method. The green dotted curve obtained with the modified contact method lies well within the range of the minimum and maximum enveloping curves obtained with the variance method for most frames of the experimental sequence. The mixing index starts at zero and eventually rises to a somewhat steady state value after about 15 seconds. All three curves reach a more or less steady mixing index estimated to around $M \approx 0.7$, indicating that a perfectly mixed state is never reached. See for instance **Fig. 9**b. The values of the original contact method are purposely not depicted as they do not form a curve but are randomly distributed across almost the entire vertical range, that is between 0 and 1 (See the supplementary materials). This wide distribution associated

with the original contact method is attributed to the image pre-processing method, which greatly reduces the number of contacts between red and white particles. A merit of the modified method, and also the variance method, is that the image preprocessing stage only has little influence in the mixing index (See Figures 10e-f).
In the experimental sequence, the value of $\bar{c}$ initially set to 0.5 increases over time and reaches a final value of $\bar{c} \approx 0.95$, as white particles move towards the inside of the drum and the front surface is mostly occupied by red particles. Adverse electrostatic effects were excluded, since preventive measures were taken, as described in Section 2.1. Experimental setup. Examination of the system after the experiment showed that no particles exhibited a charge-related behavior, such as repelling each other or resisting gravity. Therefore, this observation should solely be attributed to the contact forces between the particles and the walls, as well as their density. Preliminary DEM simulations also confirmed a higher concentration of red particles in contact with the front cap of the drum.

4 Conclusions

We have proposed a modification of the contact method encompassing a scaling of the values $C_{\min}$ and $C_{\max}$ present in the original method. This allows the quantification of mixing quality for single experimental images without necessarily having an image sequence. We have shown that our modified contact method agrees quantitatively well with the established variance method on a typical binary mixing experiment in a rotating drum, even though the variance method considers mixing from a global-statistical scope and the contact method from a local one. Our method delivers a single value for the mixing index on each image, without any parameters whose choice may be subjective. The method could be easily extended in a similar fashion to three or more granular constituents.
Our proposed modified method has some limitations in its applicability. First, a straight line is used to approximate the free surface of the particle bed in order to calculate $\tilde{L}_{\min}$. This may be a good approximation in the rolling regime or for a granular bed flowing more slowly. In the cascading regime, where the free surface exhibits a significant curvature [36], the method will likely loose applicability. Next, our modification currently works only for granular systems of uniform size and with spherical particles. Further work is needed to broaden the range of the method. Moreover, good local mixing at lower (or higher) $\bar{c}$ may lead to an overestimated global mixing index, as the method gives no information about the positions or the local density of the contacts. This is a general drawback of the contact method.

References

1. Sandadi, S., Pandey, P., Turton, R.: In situ, near real-time acquisition of particle motion in rotating pan coating equipment using imaging techniques. Chem. Eng. Sci. 59, 5807–5817 (2004). https://doi.org/10.1016/j.ces.2004.06.036
2. Silvério, B.C., Arruda, E.B., Duarte, C.R., Barrozo, M.A.S.: A novel rotary dryer for drying fertilizer: Comparison of performance with conventional configurations. Powder Technol. 270, 135–140 (2015). https://doi.org/10.1016/j.powtec.2014.10.030
3. Boateng, A.A., Barr, P. V.: Modelling of particle mixing and segregation in the transverse plane of a rotary kiln. Chem. Eng. Sci. 51, 4167–4181 (1996). https://doi.org/10.1016/0009-2509(96)00250-3
4. Yazdani, E., Hashemabadi, S.H.: DEM simulation of heat transfer of binary-sized particles in a horizontal rotating drum. Granul. Matter. 21, 1–11 (2019). https://doi.org/10.1007/s10035-018-0857-3
5. Bui, R.T., Perron, J., Read, M.: Model-based optimization of the operation of the coke calcining kiln. Carbon N. Y. 31, 1139–1147 (1993). https://doi.org/10.1016/0008-6223(93)90067-K
6. Dury, C.M., Ristow, G.H.: Competition of mixing and segregation in rotating cylinders. Phys. Fluids. 11, 1387–1394 (1999). https://doi.org/10.1063/1.870003
7. Huang, A.N., Kuo, H.P.: A study of the three-dimensional particle size segregation structure in a rotating drum. AIChE J. 58, 1076–1083 (2012). https://doi.org/10.1002/aic.12658

8. Jain, N., Ottino, J.M., Lueptow, R.M.: Regimes of segregation and mixing in combined size and density granular systems: An experimental study. Granul. Matter. 7, 69–81 (2005). https://doi.org/10.1007/s10035-005-0198-x
9. Zuriguel, I., Gray, J.M.N.T., Peixinho, J., Mullin, T.: Pattern selection by a granular wave in a rotating drum. Phys. Rev. E. 73, 061302 (2006). https://doi.org/10.1103/PhysRevE.73.061302
10. Khakhar, D. V., McCarthy, J.J., Ottino, J.M.: Radial segregation of granular mixtures in rotating cylinders. Phys. Fluids. 9, 3600–3614 (1997). https://doi.org/10.1007/s10035-011-0259-2
11. Hill, K.M., Caprihan, A., Kakalios, J.: Axial segregation of granular media rotated in a drum mixer: Pattern evolution. Phys. Rev. E. 56, 4386–4393 (1997). https://doi.org/10.1103/PhysRevE.56.4386
12. Windows-Yule, C.R.K., Scheper, B.J., van der Horn, A.J., Hainsworth, N., Saunders, J., Parker, D.J., Thornton, A.R.: Understanding and exploiting competing segregation mechanisms in horizontally rotated granular media. New J. Phys. 18, (2016). https://doi.org/10.1088/1367-2630/18/2/023013
13. Santos, D.A., Duarte, C.R., Barrozo, M.A.S.: Segregation phenomenon in a rotary drum: Experimental study and CFD simulation. Powder Technol. 294, 1–10 (2016). https://doi.org/10.1016/j.powtec.2016.02.015
14. McCarthy, J.J., Khakhar, D. V., Ottino, J.M.: Computational studies of granular mixing. Powder Technol. 109, 72–82 (2000). https://doi.org/10.1016/S0032-5910(99)00228-4
15. Rapaport, D.C.: Radial and axial segregation of granular matter in a rotating cylinder: A simulation study. Phys. Rev. E. 75, 031301 (2007). https://doi.org/10.1103/PhysRevE.75.031301
16. Yamamoto, M., Ishihara, S., Kano, J.: Evaluation of particle density effect for mixing behavior in a rotating drum mixer by DEM simulation. Adv. Powder Technol. 27, 864–870 (2016). https://doi.org/10.1016/J.APT.2015.12.013
17. Lacey, P.M.C.: Developments in the theory of particle mixing. J. Appl. Chem. 4, 257–268 (1954). https://doi.org/10.1002/jctb.5010040504
18. Fan, L.T., Chen, S.J., Watson, C.A.: Solids Mixing. Ind. Eng. Chem. 62, 53–69 (1970). https://doi.org/10.1021/ie50727a009
19. Bridgwater, J.: Mixing of powders and granular materials by mechanical means—A perspective. Particuology. 10, 397–427 (2012). https://doi.org/10.1016/j.partic.2012.06.002
20. Siiriä, S., Yliruusi, J.: Determining a value for mixing: Mixing degree. Powder Technol. 196, 309–317 (2009). https://doi.org/10.1016/j.powtec.2009.08.009
21. Chibwe, D.K., Evans, G.M., Doroodchi, E., Monaghan, B.J., Pinson, D.J., Chew, S.J.: Particle near-neighbour separation index for quantification of segregation of granular material. Powder Technol. 360, 481–492 (2020). https://doi.org/10.1016/j.powtec.2019.10.079
22. Chandratilleke, G.R., Yu, A.B., Bridgwater, J., Shinohara, K.: A particle-scale index in the quantification of mixing of particles. AIChE J. 58, 1099–1118 (2012). https://doi.org/10.1002/aic.12654
23. Asmar, B.N., Langston, P.A., Matchett, A.J.: A generalised mixing index in distinct element method simulation of vibrated particulate beds. Granul. Matter. 4, 129–138 (2002). https://doi.org/10.1007/s10035-002-0112-8
24. Lacey, P.M.C.: The mixing of solid particles. Trans. Inst. Chem. Eng. 21, 53–59 (1943). https://doi.org/10.1016/S0263-8762(97)80004-4
25. Van Puyvelde, D.R., Young, B.R., Wilson, M.A., Schmidt, S.J.: Experimental determination of transverse mixing kinetics in a rolling drum by image analysis. Powder Technol. 106, 183–191 (1999). https://doi.org/10.1016/S0032-5910(99)00074-1
26. Chou, S.-H., Song, Y.-L., Hsiau, S.-S.: A Study of the Mixing Index in Solid Particles. KONA Powder Part. J. 34, 275–281 (2017). https://doi.org/10.14356/kona.2017018
27. Gosselin, R., Duchesne, C., Rodrigue, D.: On the characterization of polymer powders mixing dynamics by texture analysis. Powder Technol. 183, 177–188 (2008). https://doi.org/10.1016/j.powtec.2007.07.021
28. Liu, X., Zhang, C., Zhan, J.: Quantitative comparison of image analysis methods for particle mixing in rotary drums. Powder Technol. 282, 32–36 (2015).

https://doi.org/10.1016/j.powtec.2014.08.076
29. Cundall, P.A., Strack, O.D.L.: A discrete numerical model for granular assemblies. Géotechnique. 29, 47–65 (1979). https://doi.org/https://doi.org/10.1680/geot.1979.29.1.47
30. Haralick, R.M., Sternberg, S.R., Zhuang, X.: Image Analysis Using Mathematical Morphology. IEEE Trans. Pattern Anal. Mach. Intell. PAMI-9, 532–550 (1987). https://doi.org/10.1109/TPAMI.1987.4767941
31. Qi, F., Heindel, T.J., Wright, M.M.: Numerical study of particle mixing in a lab-scale screw mixer using the discrete element method. Powder Technol. 308, 334–345 (2017). https://doi.org/10.1016/j.powtec.2016.12.043
32. Chou, S.H., Liao, C.C., Hsiau, S.S.: The effect of interstitial fluid viscosity on particle segregation in a slurry rotating drum. Phys. Fluids. 23, (2011). https://doi.org/10.1063/1.3623275
33. Dodge, Y. ed: The Oxford Dictionary of Statistical Terms. Oxford University Press, New York (2003)
34. Casella, G., Berger, R.L.: Statistical Inference. Duxbury Thomson Learning (2002)
35. Pratt, V.: Direct least-squares fitting of algebraic surfaces. In: Proceedings of the 14th annual conference on Computer graphics and interactive techniques - SIGGRAPH ’87. pp. 145–152. ACM Press, New York, New York, USA (1987)
36. Mellmann, J.: The transverse motion of solids in rotating cylinders—forms of motion and transition behavior. Powder Technol. 118, 251–270 (2001). https://doi.org/10.1016/S0032-5910(00)00402-2

Appendix A: Modified filling height as a function of time

The modified filling height $\tilde{h}$, normalized with the theoretical initial value $h = 53\ \mathrm{mm}$, is depicted for each image of the experimental sequence in **Fig. 13**. The modified height $\tilde{h}$ is higher by up to two particle diameters than its theoretical counterpart, which would be achieved if all particles were distributed inside the drum so that the free surface would form a perfect plane.

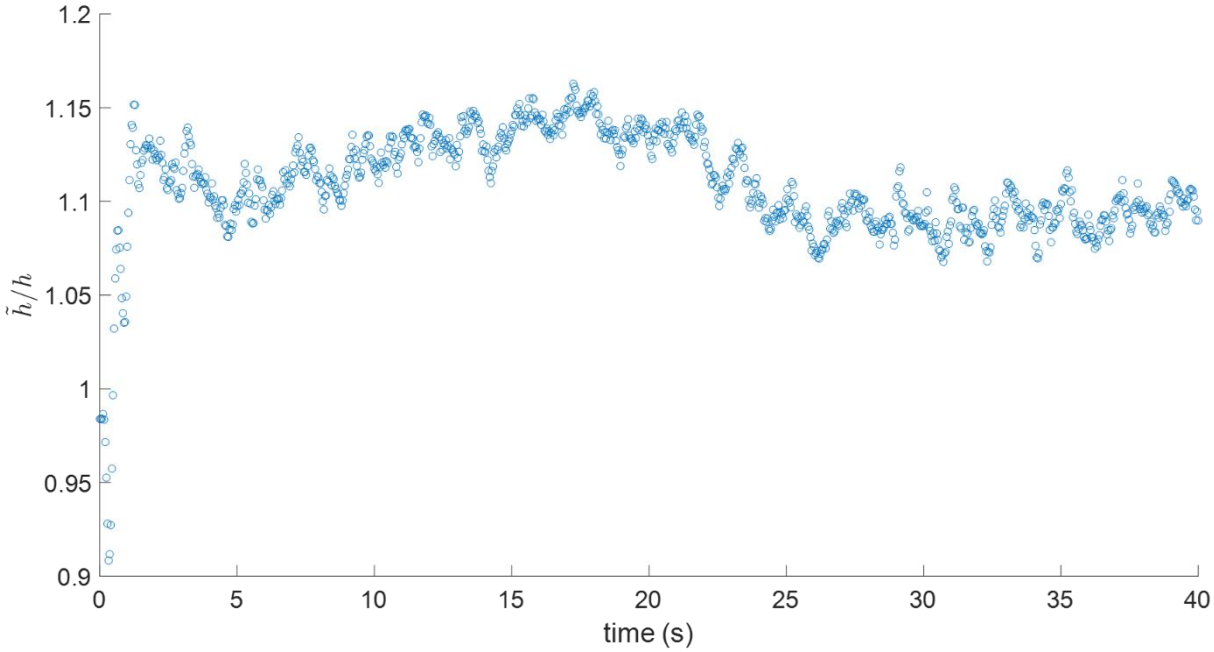

Fig. 13 *The modified filling height, $\tilde{h}$, normalized with the theoretical initial value h, as a function of time*

Appendix B: Definition of the function $\tilde{A}_R(\tilde{\ell})$ used in Eq. (13).

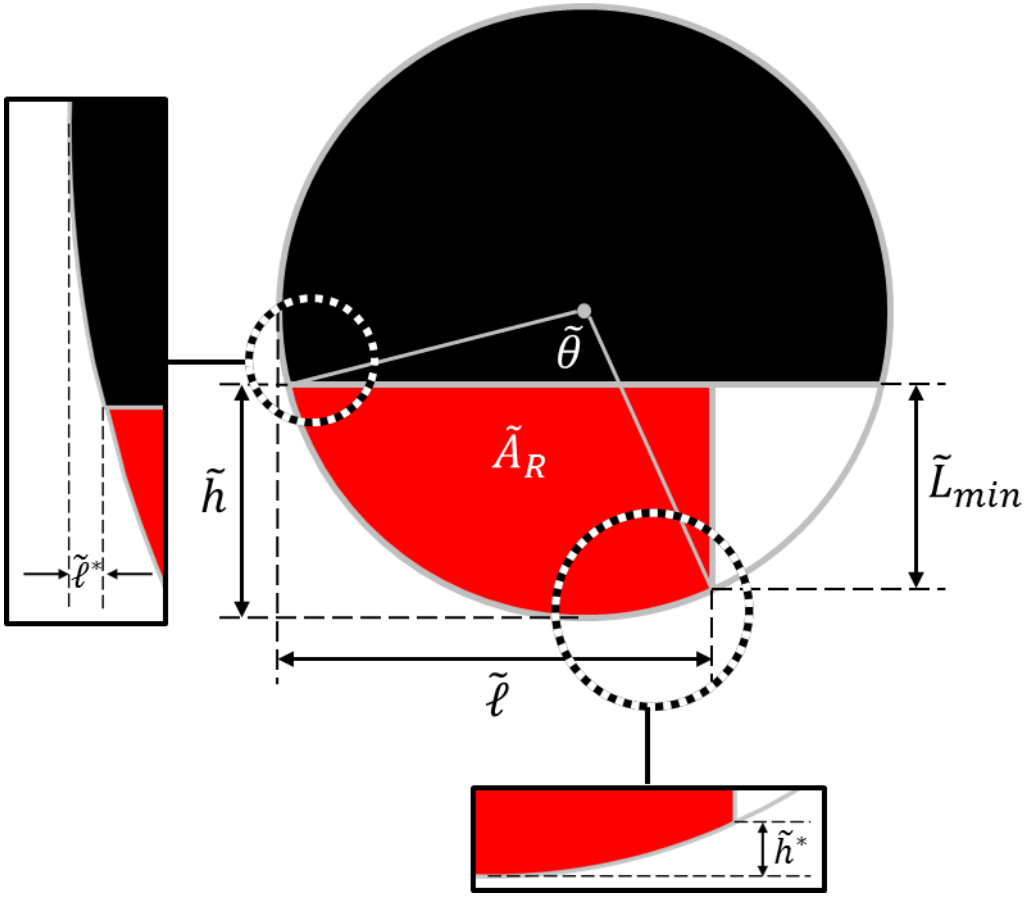

Fig. 14 *Diagram illustrating the calculation of* $\tilde{\ell}$

The modified red granular area ($\tilde{A}_R$) in Equation (13) and better illustrated in **Fig. 14** is expressed as a function of the horizontal length ($\tilde{\ell}$). Using Green's theorem, one obtains

$$\tilde{A}_R(\tilde{\ell}) = \frac{\tilde{\ell}}{2}(\tilde{h} - \tilde{h}^*) + \frac{\tilde{h}}{2}(\tilde{\ell} - \tilde{\ell}^*) + \frac{\widetilde{D}}{4}(\tilde{h}^* - \tilde{h} + \tilde{\ell}^* - \tilde{\ell}) + \frac{\widetilde{D}^2}{8}\tilde{\theta}, \tag{15}$$

where $\tilde{h}^* = \widetilde{D}/2 - \sqrt{\tilde{\ell}(\widetilde{D} - \tilde{\ell})}$, $\tilde{\ell}^* = \widetilde{D}/2 - \sqrt{\tilde{h}(\widetilde{D} - \tilde{h})}$, $\tilde{\theta} = \pi - \cos^{-1}(2\tilde{\ell}/\widetilde{D} - 1) + \sin^{-1}(2\tilde{h}/\widetilde{D} - 1)$. $\tilde{A}_R$ is defined for $\tilde{\ell}^* \le \tilde{\ell} \le \widetilde{D} - \tilde{\ell}^*$.